



INTERACTIVE EFFECTS OF CO₂, TEMPERATURE, IRRADIANCE, AND NUTRIENT LIMITATION ON THE GROWTH AND PHYSIOLOGY OF THE MARINE CYANOBACTERIUM *SYNECHOCOCCUS* (CYANOPHYCEAE)¹

Edward A. Laws ,² and S. Alex McClellan 

Department of Environmental Sciences, Louisiana State University, Baton Rouge, Louisiana, 70803, USA

The marine cyanobacterium *Synechococcus elongatus* was grown in a continuous culture system to study the interactive effects of temperature, irradiance, nutrient limitation, and the partial pressure of CO₂ (pCO₂) on its growth and physiological characteristics. Cells were grown on a 14:10 h light:dark cycle at all combinations of low and high irradiance (50 and 300 μmol photons · m⁻² · s⁻¹, respectively), low and high pCO₂ (400 and 1000 ppmv, respectively), nutrient limitation (nitrate-limited and nutrient-replete conditions), and temperatures of 20–45°C in 5°C increments. The maximum growth rate was ~4.5 · d⁻¹ at 30–35°C. Under nutrient-replete conditions, growth rates at most temperatures and irradiances were about 8% slower at a pCO₂ of 1000 ppmv versus 400 ppmv. The single exception was 45°C and high irradiance. Under those conditions, growth rates were ~45% higher at 1000 ppmv. Cellular carbon:nitrogen ratios were independent of temperature at a fixed relative growth rate but higher at high irradiance than at low irradiance. Initial slopes of photosynthesis–irradiance curves were higher at all temperatures under nutrient-replete versus nitrate-limited conditions; they were similar at all temperatures under high and low irradiance, except at 20°C, when they were suppressed at high irradiance. A model of phytoplankton growth in which cellular carbon was allocated to structure, storage, or the light or dark reactions of photosynthesis accounted for the general patterns of cell composition and growth rate. Allocation of carbon to the light reactions of photosynthesis was consistently higher at low versus high light and under nutrient-replete versus nitrate-limited conditions.

Key index words: acclimation; algal model; climate change; excretion; relative growth rate

Abbreviations: DIC, dissolved inorganic carbon; PC, particulate carbon; P–E, photosynthesis versus

irradiance; PN, particulate nitrogen; PQ, photosynthetic quotient

Cyanobacteria of the genera *Synechococcus* and *Prochlorococcus* are the most abundant marine picoplankton and are estimated to account for as much as 50% of photosynthetic carbon fixation in some regions of the ocean (Li 1994, Veldhuis et al. 1997, Zwirgmaier et al. 2008). *Synechococcus* is found from the equator to the polar circles, and it tends to be the dominant picoplankton in coastal waters and in temperate/mesotrophic waters of the open ocean (Partensky et al. 1999b). *Synechococcus* is often confined to the upper half of the euphotic zone (Partensky et al. 1999a), whereas *Prochlorococcus* is most abundant in the lower part of the euphotic zone. The fact that the principal light-harvesting pigments of *Prochlorococcus* are divinyl chlorophylls *a* and *b* (Goericke and Repeta 1992) distinguishes it from other cyanobacteria, including *Synechococcus*, which relies primarily on phycobilisomes to harvest light (Mackey et al. 2013).

There is considerable phenotypic and genotypic variability within both the *Prochlorococcus* and *Synechococcus* genera. Based on a mapping of the distributions of 10 *Synechococcus* clades in the Atlantic and Pacific oceans, Sohm et al. (2016) have concluded that the *Synechococcus* clades partition the ocean into four distinct regimes based on temperature and the concentrations of macronutrients and iron. Several studies of the effects of environmental conditions on the growth and physiology of *Synechococcus* have included the effects of temperature (Agawin et al. 1998, Mackey et al. 2013), temperature and light (Moore et al. 1995), temperature and CO₂ (Fu et al. 2007), nutrients and light (Ruan et al. 2018), and temperature, light, and nutrients (Zwirgmaier et al. 2008). However, no study has looked at the direct and interactive effects of simultaneous changes of temperature, light, CO₂ partial pressure (pCO₂), and nutrient limitation. By the year 2100, the pCO₂ in the atmosphere is expected to have risen to 700–1000 ppmv, primarily as a result of fossil fuel consumption (Houghton et al. 2001). The anticipated impacts on the surface waters of the ocean include a decrease in

¹Received 28 January 2022. Accepted 24 June 2022.

²Author for correspondence: e-mail edlaws@lsu.edu
Editorial Responsibility: J. Raven (Associate Editor)

the pH by 0.3 (Yool et al. 2013) and an increase in sea surface temperature by 1–4°C (Feng et al. 2009). The increase in thermal stratification is expected to lead to a shoaling of the mixed layer that will increase the average irradiance to which phytoplankton in the mixed layer are exposed (Gao et al. 2012a,b, Hutchins and Fu 2017) and increase the degree of nutrient limitation by reducing the influx of nutrients through the nutricline (Rost et al. 2008, Beardall et al. 2009). Thus, climate change effects are expected to cause simultaneous changes of the physicochemical environment of the mixed layer in terms of temperature, irradiance, pCO₂, pH, and the supply of inorganic nutrients.

The present study was undertaken to determine the direct effects and interactive effects of such simultaneous changes on a species of the genus *Synechococcus*. We chose a clone of *S. elongatus* that grew well over a wide temperature range (20–45°C) to facilitate studies of interactions between temperature and other environmental variables. The experimental design enabled us to test several hypotheses: (i) The nutrient-replete growth rates of *S. elongatus* are unaffected by changing the pCO₂ from 400 ppmv to 1000 ppmv. Fu et al. (2007) have reported that raising the pCO₂ from 380 to 750 ppmv has no significant effect on the growth rate of *Synechococcus* CCMP 1334 at 20 and 24°C and a fixed irradiance. We are not aware of any studies that have tested for effects of pCO₂ on growth rates over a wide range of temperatures and at more than one irradiance; (ii) if pCO₂ affects the growth rates of *S. elongatus* under nutrient-replete conditions, the effects are independent of temperature and irradiance; (iii) the physiological condition of *S. elongatus* as evidenced by the initial slope and asymptote of short-term photosynthesis–irradiance curves is independent of temperature, irradiance, nutrient-limitation status, and pCO₂; (iv) the carbon:nitrogen (C:N) ratio of *S. elongatus* cells is a unique function of their relative growth rate (i.e., the ratio of their nutrient-limited growth rate to their growth rate under nutrient-replete but otherwise identical conditions). This is an hypothesis that Goldman (1980) originally proposed would apply to all phytoplankton, but to our knowledge, it has not been tested over a range of temperatures, different irradiances, or different partial pressures of CO₂ for any species; and (v) variations of the C:N ratios and carbon:chlorophyll *a* (C:Chl *a*) ratios of *S. elongatus* are independent of pCO₂ and can be explained as functions of temperature, irradiance, and degree of nutrient limitation by a simple model of carbon allocation in phytoplankton based on the pioneering work of Shuter (1979).

MATERIALS AND METHODS

Culturing conditions. The culture of *Synechococcus elongatus* was obtained from the National Center for Marine Algae

and Microbiota (strain CCMP 1629) and had been originally isolated from a mangrove pool near Goleta, Panama. *Synechococcus elongatus* was grown in a continuous culture system identical to that described by Laws et al. (2020) except for the growth chamber, which was made of polycarbonate (Fig. S1 in the Supporting Information) rather than glass. Our experience with *Synechococcus* has been that it grows well in a glass growth chamber in batch mode but washes out in continuous mode (Popp et al. 1998). The washout problem is easily overcome if the growth chamber is made of polycarbonate rather than glass. The experiments were conducted from January 2016 through March 2020 and included a total of 48 steady states at six temperatures (20, 25, 30, 35, 40, and 45°C), low and high irradiance (50 and 300 μmol photons · m⁻² · s⁻¹, respectively), low and high pCO₂ (400 and 1000 ppmv, respectively), and either nitrate-limited or nutrient-replete growth conditions. Details of the experimental procedures can be found in Appendix S1 in the Supporting Information. Briefly, the growth chamber was a double-walled system that consisted of one polycarbonate bottle with a working volume of 1130 mL inside another larger polycarbonate bottle. Temperature was controlled to within ±0.1°C by circulating water from a thermoregulated water bath (Haake Model DC10) through the space between the outer wall of the growth chamber and the larger surrounding polycarbonate bottle. A complete set of experiments was carried out in 5°C increments from 20°C to 45°C under nutrient-replete conditions at both high and low irradiance and high and low pCO₂ (a total of 24 steady states) to determine, inter alia, the growth rates of the cells under nutrient-replete conditions for each combination of temperature, irradiance, and pCO₂. Light was provided by a bank of daylight fluorescent lamps on a 14:10 h light:dark cycle of illumination. The irradiance was measured at the center of the empty growth chamber with a quantum scalar light meter (Biospherical Instruments Model QSL 2100, San Diego, CA, USA). The irradiance so measured was either 50 or 300 μmol photons · m⁻² · s⁻¹ of photosynthetically active radiation (400–700 nm wavelength). The former irradiance was achieved by placing neutral density screens between the light source and the growth chamber. The growth medium consisted of artificial seawater enriched with vitamins and inorganic nutrients sufficient to produce a salinity of 35 and a total alkalinity of 2.4 meq · kg⁻¹. Trace metals were added in an EDTA-buffered solution as specified by Sunda and Hardison (2007). The nitrate concentrations in the growth medium used for the nitrate-limited and nutrient-replete studies were 20 μM and 882 μM, respectively. Concentrations of phosphate and vitamins were identical to those specified for f/2 medium; silicate was omitted. The growth chamber and 40 L medium reservoir were sterilized by autoclaving, and the growth medium was sterile-filtered (0.2 μm) into the reservoir. Fresh medium was introduced into the growth chamber at a controlled rate via a peristaltic pump. The culture was stirred by a Teflon-coated magnetic stir bar and via bubbling with sterile air (0.2 μm sterile filter), which also served to drive the overflow by pressurizing the headspace above the culture. The pCO₂ in the growth chamber was controlled by bubbling sterile air admixed with regulated amounts of pure CO₂ (Bone Dry 3.0 Grade) through the medium in the nutrient reservoir and from there into the growth chamber. The pCO₂ of the inflow air was monitored continuously by an infrared absorption-based CO₂ meter (AZ-0004; CO2meter.com).

Inorganic carbon system. The pH and total alkalinity of the growth chamber were monitored shortly after the start of the photoperiod, the middle of the photoperiod, and shortly before the end of the photoperiod. The pH was measured on the total hydrogen ion scale based on the spectrophotometric

method described in SOP 6b by Dickson et al. (2007). Absorbances for pH determination were measured in a 5 cm glass cuvette on a Spectronic Helios Delta UV-Visible spectrophotometer (Thermo Scientific, Waltham, MA, USA). Total alkalinity was determined based on the single-point titration described by Breland and Byrne (1993). Briefly, 100 mL of culture was brought to 25°C and titrated to an approximate pH of 4.0–4.3 with standardized HCl (Fisher) diluted to 0.10 N in 0.6 M NaCl. The solution was stirred vigorously during the titration and for 5 min continuously. Approximately 0.5 mL of 2 mM bromocresol green (pH 4.2) was then added to the titrated solution. The precise endpoint pH of the resultant solution was then determined based on its absorbance at 750, 616, and 444 nm using the same configuration as for the pH measurements (above). The dissolved inorganic carbon (DIC) concentration was calculated based on pH and total alkalinity using the equations and equilibrium constants published in Zeebe and Wolf-Gladrow (2001). The pCO₂ in the growth chamber was calculated based on the DIC concentration and total alkalinity in accord with EU (2011) using the CO2calc software package (Robbins et al. 2010). Table S1 in the Supporting Information summarizes the characteristics of the growth medium as a function of temperature and pCO₂.

Sampling and analysis. The optical density of the culture was recorded at the same time of day each day during the light period. A sample of the culture was placed in a 5 cm cuvette, and the extinction coefficient at 750 nm was measured with a Spectronic Helios model Delta spectrophotometer (Thermo Fisher). Dilution rates were recorded at the same time. Sampling of the growth chamber for characteristics other than optical density did not begin until four doubling times (i.e., generation times) had elapsed at each dilution rate, by which time the optical density had stabilized with a coefficient of variation of ±2%. Growth rates in continuous cultures are equal to the dilution rates once cell concentrations have stabilized. Once begun, sampling for chlorophyll *a* (Chl *a*) and for particulate carbon (PC) and particulate nitrogen (PN) was done immediately after the start of the photoperiod and just before the end of the photoperiod. The experimental design was expected to reveal effects of acclimation but not of adaptation (e.g., Li et al. 2017). Samples were collected via a three-way valve (Fig. S2 in the Supporting Information); they were not collected from the growth chamber overflow. The growth chamber was always overflowing when a sample was withdrawn (i.e., the interval between two consecutive samples was always long enough to allow the volume removed for one sample to be replaced before the next sample was withdrawn). Samples for determination of PC, PN, and Chl *a* were collected on glass fiber filters (GF/F; Whatman). Concentrations of Chl *a* were measured in methanol extracts on a Cary model 50 UV-Visible spectrophotometer (Agilent Technologies, Maidstone, United Kingdom and Santa Clara, CA, USA) using the protocol of Holm-Hansen and Riemann (1978). PC and PN were measured on an elemental analyzer (model CE 440; Exeter Analytical, Chelmsford, MA, USA).

Rates of PC production in the growth chamber during the photoperiod were calculated by integrating the differential equation:

$$\frac{d(\text{PC})}{dt} = \Pi - \mu \cdot \text{PC} \quad (1)$$

where Π is the rate of PC production (mg C · h⁻¹), and μ is the dilution rate per hour. If Π is constant during the photoperiod, the solution to eq. 1 is

[Correction added on 16 August 2022, after first online publication: ‘t’ has been replaced by ‘μ’ on several occasions in this version].

$$\text{PC}_{14} = \text{PC}_0 e^{-14\mu} + \frac{\Pi}{\mu} (1 - e^{-14\mu}) \quad (2)$$

where PC₀ and PC₁₄ are the PC concentrations at the beginning and end of the 14 h photoperiod, respectively. The rate of photosynthesis during the photoperiod was then estimated from eq. 3:

$$\Pi = \mu \left(\frac{\text{PC}_{14} - \text{PC}_0 e^{-14\mu}}{1 - e^{-14\mu}} \right) \quad (3)$$

Production rates calculated with eq. 3 were divided by the average of the Chl *a* concentrations at the beginning and end of the photoperiod to estimate the productivity index during the photoperiod in units of g C · (g Chl *a*)⁻¹ · h⁻¹.

Short-term photosynthesis versus irradiance assays. Short-term photosynthesis versus irradiance (P–E) assays were conducted based on inorganic ¹⁴C incorporation into organic matter during a 5 min incubation at multiple light intensities. For each set of conditions, a P–E assay was conducted at each of three different times during the photoperiod: within 1 h of the start of the photoperiod, at the middle of the photoperiod, and within 1 h of the end of the photoperiod. Each assay was performed using an aliquot of steady-state culture that was withdrawn via the three-way valve (Fig. S1) immediately prior to the start of each assay. Five-minute ¹⁴C uptake experiments were conducted at a series of irradiances from 5 to 400 μmol photons · m⁻² · s⁻¹ of 400–700 nm radiation measured with the QSL 2100 quantum scalar light meter.

A platform was set up in front of a bank of fluorescent lamps, and 20 mL glass vials were positioned on the platform at varying distances from the lamps to achieve the following irradiances: 5, 10, 30, 55, 80, 120, 150, 200, 300, and 400 μmol photons · m⁻² · s⁻¹. Three replicate vials were placed at each irradiance position. To account for background activity and any dark uptake, an additional three vials were wrapped in aluminum foil but otherwise treated in the same manner as the exposed vials. Details are provided in Appendix S1. At each irradiance, the fraction of the total DIC that was incorporated during the 5 min incubation at irradiance *E* (fDIC_E) was calculated with eq. 4:

$$\text{fDIC}_E = \frac{\bar{A}_E - \bar{A}_0}{\bar{A}_T - \bar{A}_B} \times 1.05 \quad (4)$$

where \bar{A}_E and \bar{A}_0 represent the average ¹⁴C activity (counts per min) at irradiance *E* and irradiance 0, respectively, and \bar{A}_T and \bar{A}_B represent that of the total ¹⁴C addition and background activity, respectively; 1.05 is the assumed isotopic discrimination factor for ¹⁴C. Within 15 min of each P–E assay, duplicate 50 mL aliquots of the culture were filtered onto GF/F filters for Chl *a* quantification as described above. The DIC of the culture at the time of sampling for each assay was determined as described above.

The photosynthetic rate normalized to Chl *a* at each irradiance (P_E^*) was calculated based on fDIC_E and the concentrations of DIC (g C · L⁻¹) and Chl *a* (g Chl *a* · L⁻¹) as shown in eq. 5, where 12 converts the 5 min incubation period to an hourly basis so that P_E^* is in units of g C · (g Chl *a*)⁻¹ · h⁻¹.

$$P_E^* = \frac{\text{fDIC}_E \times \text{DIC}}{\text{Chl } a} \times 12 \quad (5)$$

The data were fit by a nonlinear least squares regression (MATLAB, R2016b) based on a hyperbolic tangent model (eq. 6; Fig. S3 in the Supporting Information), where P_{max}^* is

the light-saturated photosynthetic rate, and α is the slope of the uptake curve in the limit as $E \rightarrow 0$.

$$P_E^* = P_{\max}^* \tanh\left(\frac{E\alpha}{P_{\max}^*}\right) \quad (6)$$

Model. We used the theoretical model of Laws and Chalup (1990) to try to explain the response of *Synechococcus elongatus* to changes of environmental conditions. Appendix S1 provides a detailed description of the model, which is a modification of an earlier model by Shuter (1979). Briefly, the carbon in the cell is assumed to be allocated to structure (S), storage (R), the light reactions of photosynthesis (P), or the dark reactions of photosynthesis (E). The allocation to structure is assumed to be a fixed proportion of the cell carbon. The rates of the light and dark reactions of photosynthesis are assumed to equal one another. The rate of the light reactions is assumed to be a saturating function of irradiance (e.g., eq. 6), and the rate of the dark reactions is assumed to be an empirically determined function of temperature. The cells are assumed to allocate carbon in a way that maximizes their growth rate. The requirement for equality of the rates of the light and dark reactions of photosynthesis leads to a quadratic equation, and the requirement that the growth rate be maximized is satisfied by only one root of the quadratic equation. The composition of the cells is thus uniquely determined as a function of environmental conditions.

Composition of accessory pigments relative to Chl a. To determine how nitrate and light limitation affected the abundance of total carotenoids and phycobilins relative to Chl *a* in CCMP 1629, we measured the concentrations of Chl *a*, total carotenoids, and the phycobilins phycocyanin and allophycocyanin in chemostat cultures that were growing at 25°C under a pCO₂ of 400 ppmv. Replicate 100 mL samples were collected during mid-photoperiod at each of the four combinations of nutrient-replete or nitrate-limited conditions at low and high irradiance (50 and 300 μmol photons · m⁻² · s⁻¹, respectively). Upon collection, each replicate sample was equally divided between two 50 mL centrifuge tubes (one for extraction of Chl *a* and carotenoids, and the other for extraction of phycobilins). The tubes were immediately centrifuged at 3500g for 10 min to pellet the cells. After the supernatant was discarded, the cell pellets were stored frozen at -20°C until pigment extraction. Chl *a* and the carotenoids were extracted together in methanol. Chl *a* was quantified as described above. The concentration of total carotenoids was estimated based on the method of Strickland and Parsons (1972), that is, the absorbance at 480 nm assuming an extinction coefficient of 0.25 mL · μg⁻¹ · cm⁻¹. Phycocyanin and allophycocyanin were extracted in a freshly prepared aqueous lysozyme buffer as per Ruan et al. (2018) with modifications. The buffered solution (pH 7.0) contained 10 mM sodium phosphate, 150 mM NaCl, and 10 mg · mL⁻¹ lysozyme. The cell pellets were resuspended in 10–25 mL of the lysozyme buffer and incubated at 37 ± 2°C for 14 h. For CCMP 1629, we found that the greater concentration of lysozyme (10 vs. 5 mg · mL⁻¹) and longer incubation time (14 vs. 2 h) than those used by Ruan et al. (2018) were necessary to completely lyse the cells. After extraction, the lysates were centrifuged at 3500 g for 10 min. The concentrations of phycocyanin and allophycocyanin in the supernatants were quantified spectrophotometrically using the equations and extinction coefficients determined by Bennett and Bogorad (1973). We refer to the quantities of phycocyanin and allophycocyanin collectively as the quantity of phycobilins; phycoerythrin was not detected in any of the samples.

DNA sequencing of the ITS region of CCMP 1629. To determine the taxonomic cluster of *Synechococcus* to which CCMP 1629 might belong, we performed Sanger sequencing of the 16S–23S internal transcribed spacer (ITS) region of the ribosomal DNA of

this strain. Two milliliters of log-phase culture of CCMP 1629 was centrifuged at 10,000g for 5 min to pellet the cells. After discarding the supernatant, the cell pellet was resuspended in 400 μL of a Tris-buffered lysozyme solution (pH 8.0) that contained 100 mM NaCl, 10 mM Tris, 1 mM EDTA, and 10 mg · mL⁻¹ lysozyme. The suspension was incubated at 37 ± 2°C overnight to lyse the cells. Four microliters of 100-mg · mL⁻¹ RNase A solution (Qiagen) was then added to the cell lysate, which was then incubated at 65 ± 2°C for 10 min. The DNA was isolated from the lysate by column purification using the Qiagen DNeasy Plant Mini kit following the manufacturer's instructions but beginning with Step 9 (addition of neutralization buffer P3). The DNA was eluted in 50 μL of the supplied elution buffer (10 mM Tris-Cl, 0.5 mM EDTA). DNA purity and integrity were confirmed based on UV absorbance (Thermo Fisher NanoDrop 2000c) and agarose gel electrophoresis, respectively.

The ITS region of the ribosomal DNA, including part of the proximal 16S and 23S rDNA gene regions, was amplified by PCR as per Ahlgren and Rocap (2012) using the primers 23S-241R (5'-TTCGCTCGCCRCTACT-3') and a modified version of 16S-1247F (Syn7002-1247F: 5'-CGTACTACAATGGTC GGG-3'). The three-base modification to the 16S-1247F primer sequence was made because no amplification was observed for CCMP 1629 using the original sequence. The modified sequence was designed to match the corresponding sequence of PCC 7002, a strain to which CCMP 1629 appears physiologically similar in terms of its optimal growth conditions. The PCR was carried out in triplicate in a total volume of 50 μL containing 200 ng of template DNA, 0.5 μM of each primer, and 25 μL of GoTaq Green 2X Master Mix (Promega; 400 μM of each dNTP and 3 mM MgCl₂). Reaction cycling was done using a Mastercycler Gradient thermocycler (Eppendorf Scientific, Enfield, Connecticut, USA) following the reaction conditions of Ahlgren and Rocap (2012). The ~1 kbp amplicon was column-purified using the Qiagen QIAquick PCR Purification kit and eluted in Tris/low-EDTA buffer (10 mM Tris, 0.05 mM EDTA). One-hundred and fifty nanograms of the purified product was electrophoresed in 1.8% agarose gel (50 mM sodium borate, pH 8.5) at 20 V · cm⁻¹ to confirm the removal of primers and the presence of only one amplicon.

Sequencing of the amplicon was performed in triplicate in both directions using four primers: Syn7002-1247F, 23S-241R, and two internal primers ITS-AlaF (5'-TWTAGCTCAGTTGGT AGAG-3') and ITS-AlaR (5'-CTCTACCAACTGAGCTAWA-3'; Rocap et al. 2002). The sequencing reaction, post-reaction purification, and electrophoresis were performed by the LSU Genomics Facility. Each 10 μL reaction volume contained 0.5 μL of BigDye Terminator v3.1 mix (Applied Biosystems Inc., San Francisco, California, USA), 3.5 μL of BigDye 5X sequencing buffer, 2 μM primer, and 6 ng of template. The reaction cycling conditions were as follows: 95°C for 60 s, followed by 25 cycles of 95°C for 10 s, 50°C for 5 s, 55°C for 5 s, and 60°C for 2 min. The sequencing products were purified by ethanol precipitation and resuspended in 15 μL of Hi-Di formamide. Electrophoresis and base calling were performed on an ABI 3130XL Genetic Analyzer (Applied Biosystems Inc.). The trace scores for all samples exceeded 55, and the contiguous read lengths ranged from 457 to 732 bases. Within each set of triplicate sequences, there was no more than a single base mismatch, and at least two of the three were always identical. The sequences yielded by each primer were aligned using the GeneDoc v2.7 application (Nicholas and Nicholas 1997), and a consensus sequence for the whole ITS region was generated. The resultant sequence was queried against the NCBI GenBank standard nucleotide database (<https://www.ncbi.nlm.nih.gov/genbank/>) using the BLAST search tool. The results of the query were ranked according to % coverage and identity relative to the CCMP 1629 sequence.

RESULTS

Table S2 in the Supporting Information provides a summary of the results obtained at all 48 growth conditions. Although the growth chamber was continuously bubbled with air containing either 400 or 1000 ppmv pCO₂, the pCO₂ in the growth medium varied systematically during the light:dark cycle because of photosynthetic uptake and respiratory release of CO₂. When the pCO₂ in the air was 400 ppmv, the pCO₂ in the growth chamber varied between no less than 300 (end of photoperiod) and no more than 500 ppmv (beginning of photoperiod). When the pCO₂ in the air was 1000 ppmv, the pCO₂ in the growth chamber varied between no less than 800 (end of photoperiod) and no more than 1200 ppmv (beginning of photoperiod).

Under nutrient-replete conditions, the growth rates of *Synechococcus elongatus* ranged from $\sim 0.6 \cdot \text{d}^{-1}$ at 20°C and low irradiance to $\sim 4.5 \cdot \text{d}^{-1}$ at 30–35°C and high irradiance (Fig. 1). Temperatures of 20 and 25°C were clearly suboptimal, and 45°C was clearly supraoptimal. The effect of temperature on the growth rates was more dramatic at high irradiance than at low irradiance because light absorption, which becomes increasingly rate-limiting as the irradiance is reduced, is independent of temperature. The cells grew more rapidly at 400 ppmv than at 1000 ppmv pCO₂ (sign test, 11 of 12

comparisons, $P = 0.006$). Our first hypothesis that the nutrient-replete growth rates of *S. elongatus* would be unaffected by changing the pCO₂ from 400 ppmv to 1000 ppmv was therefore false. The nutrient-replete growth rates were higher at 400 ppmv than at 1000 ppmv pCO₂.

To test our second hypothesis that the effects of pCO₂ on the nutrient-replete growth rates were independent of temperature and irradiance, we first calculated the ratios of the nutrient-replete growth rates at 1000 ppmv pCO₂ to the analogous growth rates at 400 ppmv pCO₂ for high and low irradiance separately and calculated the correlation coefficients between the ratios and temperature. We ran the correlation tests with three correlation coefficients: Pearson, Spearman, and Kendall. In all cases, the correlations between the ratios and temperature were not significant ($r_{p,4} = 0.66$, $P = 0.15$; $r_{s,4} = 0.43$, $P = 0.42$; $r_{k,4} = 0.47$, $P = 0.27$). We then performed a paired t -test of the ratios at high and low irradiance for the six different temperatures. There was no significant difference ($t_5 = 0.52$, $P = 0.63$) of the ratios at high and low irradiance. The median ratio of the growth rates at high and low pCO₂ for all six temperatures and high and low irradiance was 0.92 with 95% confidence limits of 0.87–0.98. The lone exception to this pattern was the ratio of growth rates at 45°C and high irradiance. In that

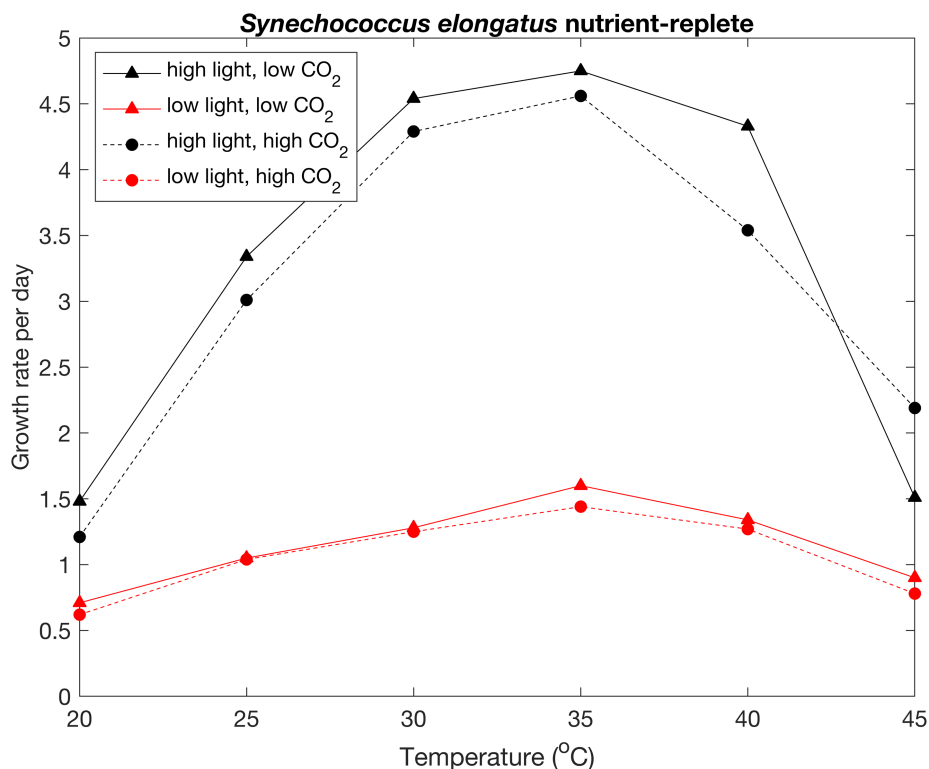


FIG. 1. Net growth rates of *Synechococcus elongatus* grown on a 14:10 h light:dark cycle under nutrient-replete conditions, high or low irradiance (300 or 50 $\mu\text{mol photons} \cdot \text{m}^{-2} \cdot \text{s}^{-1}$, respectively), and either high or low pCO₂ (1000 or 400 ppmv, respectively).

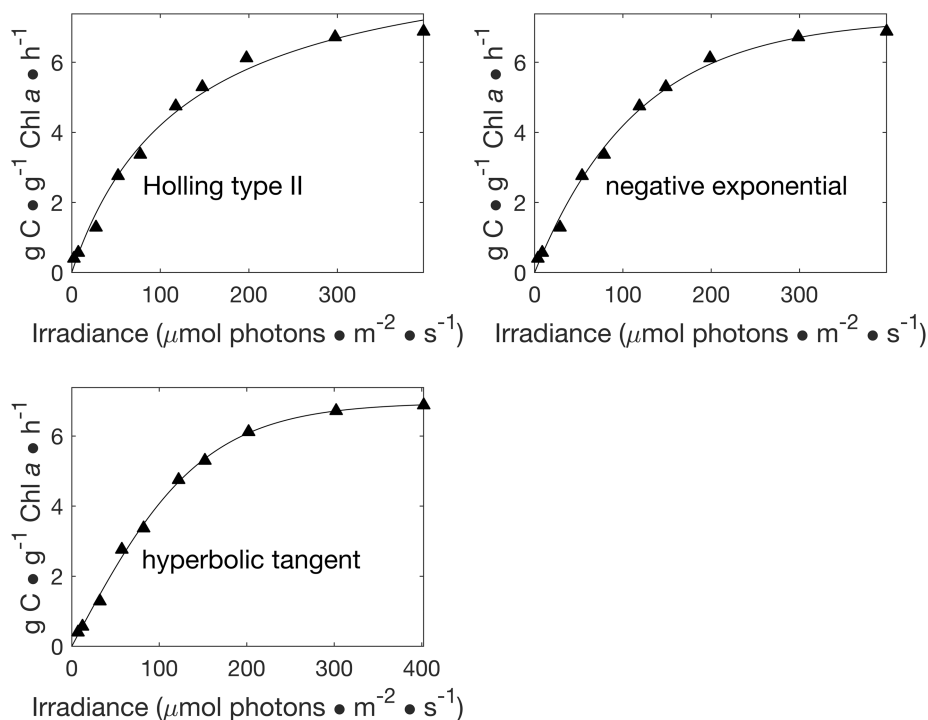


FIG. 2. Results of fitting a 5 min photosynthesis versus irradiance curve to Holling type II (rectangular hyperbola), negative exponential, and hyperbolic tangent functions. This experiment was carried out in the middle of the photoperiod under nitrate-limited conditions, 45°C, irradiance of 50 $\mu\text{mol photons} \cdot \text{m}^{-2} \cdot \text{s}^{-1}$, and 1000 ppmv pCO_2 .

case, the growth rate was 45% higher at 1000 ppmv than at 400 ppmv.

Figure 2 shows the results of a 5 min ^{14}C uptake experiment conducted shortly after the start of the photoperiod under nitrate-limited conditions, 45°C, an irradiance of 50 $\mu\text{mol photons} \cdot \text{m}^{-2} \cdot \text{s}^{-1}$, and 1000 ppmv pCO_2 . Comparisons of the goodness of fit of a Holling type II function (rectangular hyperbola), negative exponential, and hyperbolic tangent to the data revealed that the hyperbolic tangent gave the best fit to the data. This result was very typical of the results of our ^{14}C uptake experiments: The hyperbolic tangent consistently gave the best fit to the data.

Figure 3 shows values of α , the initial slope of the photosynthesis–irradiance curves, as a function of temperature for cells grown under high irradiance or low irradiance (Fig. 3A) and nutrient-replete or nitrate-limited conditions (Fig. 3B). At temperatures of 25–45°C, there was no difference in α values at high irradiance ($1.3 \pm 0.15 \text{ m}^2 \cdot \text{mol C} \cdot (\text{mol photons})^{-1} \cdot (\text{g Chl } a)^{-1}$) and low irradiance ($1.2 \pm 0.08 \text{ m}^2 \cdot \text{mol C} \cdot (\text{mol photons})^{-1} \cdot (\text{g Chl } a)^{-1}$; paired t -test, $P = 0.53$), but at 20°C, the mean α was much higher at low irradiance ($1.3 \pm 0.27 \text{ m}^2 \cdot \text{mol C} \cdot (\text{mol photons})^{-1} \cdot (\text{g Chl } a)^{-1}$) than at high irradiance ($0.53 \pm 0.11 \text{ m}^2 \cdot \text{mol C} \cdot (\text{mol photons})^{-1} \cdot (\text{g Chl } a)^{-1}$). Values of α were consistently higher under nutrient-replete versus nitrate-limited conditions (paired t -test, $t_{23} = 3.9$, $P = <0.001$). Values of α were not significantly different at 400

ppmv pCO_2 and 1000 ppmv CO_2 (paired t -test, $t_{23} = 1.8$, $P = 0.08$), and they were not significantly different at low and high irradiance (paired t -test, $t_{23} = 0.31$, $P = 0.76$).

Figure 4 shows photosynthetic rates normalized to Chl a (i.e., productivity indices) as a function of temperature, irradiance, and nutrient limitation. The values in Figure 4A were calculated with eq. 3 and are therefore based on changes of the PC concentrations in the growth chamber during the photoperiod. The values in Figure 4B are P_{max}^* values (eq. 6) and are based on the results of 5 min ^{14}C uptake experiments. The P_{max}^* values are therefore asymptotic values and would be expected to exceed the corresponding productivity indices. This was true at both high irradiance (paired t -test, $t_{23} = 7.4$, $P = 1.7 \times 10^{-7}$), and low irradiance (paired t -test, $t_{23} = 6.3$, $P = 1.8 \times 10^{-6}$). The average $P_{\text{max}}^*/\text{PI}$ ratio was 1.9 ± 0.12 (mean \pm standard error, $\text{df} = 47$).

Productivity indices calculated from changes of PC concentrations were significantly higher at 400 ppmv pCO_2 ($6.1 \pm 0.9 \text{ g C} \cdot (\text{g Chl } a)^{-1} \cdot \text{h}^{-1}$) than at 1000 ppmv pCO_2 ($5.4 \pm 0.7 \text{ g C} \cdot (\text{g Chl } a)^{-1} \cdot \text{h}^{-1}$) based on a paired t -test ($t_{23} = 2.57$, $P = 0.017$) and were significantly higher at high irradiance ($9.0 \pm 0.6 \text{ g C} \cdot (\text{g Chl } a)^{-1} \cdot \text{h}^{-1}$) than at low irradiance ($2.5 \pm 0.1 \text{ g C} \cdot (\text{g Chl } a)^{-1} \cdot \text{h}^{-1}$) based on a paired t -test ($t_{23} = 11.6$, $P = 4.5 \times 10^{-11}$). Although productivity indices were significantly higher under nutrient-replete conditions ($6.4 \pm 0.9 \text{ g C} \cdot (\text{g Chl } a)^{-1} \cdot \text{h}^{-1}$) than under nitrate-limited conditions ($5.4 \pm 0.7 \text{ g C} \cdot (\text{g Chl } a)^{-1} \cdot \text{h}^{-1}$) based on a paired t -test ($t_{23} = 3.9$, $P = <0.001$), they were not significantly different at 400 ppmv pCO_2 and 1000 ppmv CO_2 (paired t -test, $t_{23} = 1.8$, $P = 0.08$), and they were not significantly different at low and high irradiance (paired t -test, $t_{23} = 0.31$, $P = 0.76$).

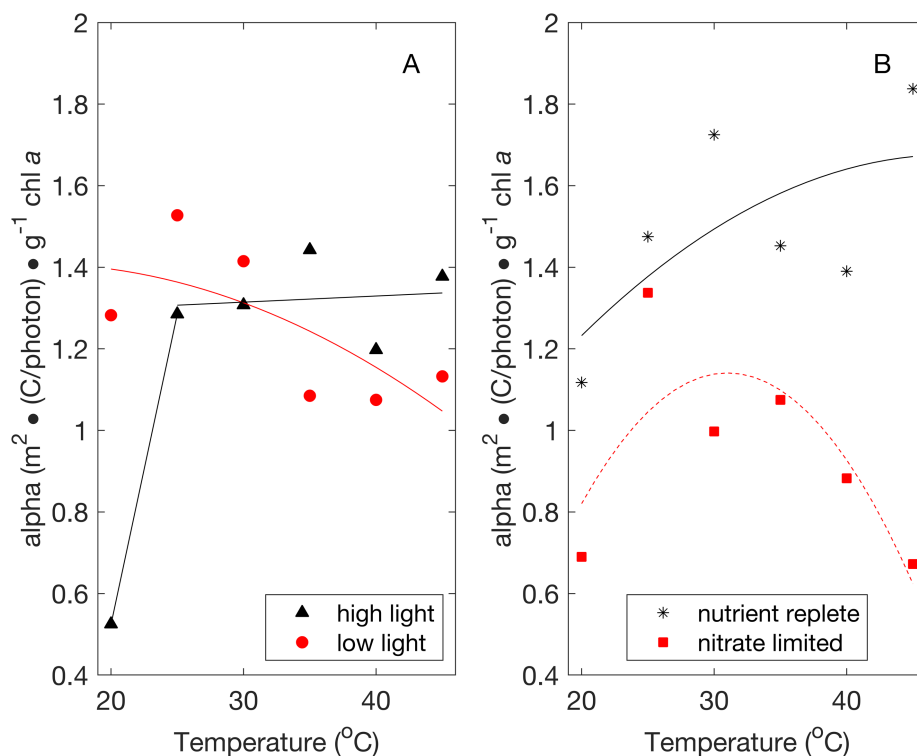


FIG. 3. Values of α , the initial slope of the photosynthesis–irradiance curves (e.g., Fig. 2) as a function of temperature. In panel A, the values are averages under high light or low light conditions. In panel B, the values are averages under nutrient-replete or nitrate-limited conditions. Lines are least squares fits of the data.

$a)^{-1} \cdot \text{h}^{-1}$) than under nitrate-limited conditions ($5.2 \pm 0.6 \text{ g C} \cdot (\text{g Chl } a)^{-1} \cdot \text{h}^{-1}$) based on a paired t -test ($t_{23} = 2.57$, $P = 0.017$), at low irradiance the productivity indices were slightly higher under nitrate-limited conditions ($2.7 \pm 0.16 \text{ g C} \cdot (\text{g Chl } a)^{-1} \cdot \text{h}^{-1}$) than under nutrient-replete conditions ($2.3 \pm 0.19 \text{ g C} \cdot (\text{g Chl } a)^{-1} \cdot \text{h}^{-1}$) based on a paired t -test ($t_{11} = 3.02$, $P = 0.01$).

The P_{max}^* values were higher at 400 ppmv pCO_2 ($10.8 \pm 1.3 \text{ g C} \cdot (\text{g Chl } a)^{-1} \cdot \text{h}^{-1}$) than at 1000 ppmv pCO_2 ($9.2 \pm 1.2 \text{ g C} \cdot (\text{g Chl } a)^{-1} \cdot \text{h}^{-1}$) based on a paired t -test ($t_{23} = 2.46$, $P = 0.06$), and they were significantly higher at high irradiance ($14.8 \pm 1.1 \text{ g C} \cdot (\text{g Chl } a)^{-1} \cdot \text{h}^{-1}$) than at low irradiance ($5.0 \pm 0.4 \text{ g C} \cdot (\text{g Chl } a)^{-1} \cdot \text{h}^{-1}$) based on a paired t -test ($t_{23} = 9.2$, $P = 6.1 \times 10^{-9}$). Although P_{max}^* values were significantly higher under nutrient-replete conditions ($11.6 \pm 1.5 \text{ g C} \cdot (\text{g Chl } a)^{-1} \cdot \text{h}^{-1}$) than under nitrate-limited conditions ($8.3 \pm 0.9 \text{ g C} \cdot (\text{g Chl } a)^{-1} \cdot \text{h}^{-1}$) based on a paired t -test ($t_{23} = 2.9$, $P = 0.005$), the difference at low irradiance was not significant (paired t -test, $t_{11} = 0.2$, $P = 0.84$).

We used the productivity indices and the rates of CO_2 uptake from the 5 min ^{14}C uptake experiments at ambient irradiance (50 or 300 $\mu\text{mol photons} \cdot \text{m}^{-2} \cdot \text{s}^{-1}$) to calculate the ratio of net photosynthesis to gross photosynthesis (= productivity index \div gross photosynthesis normalized to Chl a) and

subtracted that ratio from 1.0 to estimate the ratio of respiration in the light to gross photosynthesis (Fig. 5). Paired t -tests revealed no significant difference between these ratios at high and low irradiance ($t_{23} = 1.2$, $P = 0.26$), at high and low pCO_2 ($t_{23} = 0.48$, $P = 0.64$), and under nutrient-replete versus nitrate-limited conditions ($t_{23} = 1.9$, $P = 0.068$), but a Kruskal–Wallis test revealed a significant temperature effect (KW statistic_{5,42} = 12.3, $P = 0.03$). We therefore averaged the eight ratios at each temperature to estimate respiration rates in the light at each temperature (Fig. 5). The average ratio was a minimum at 35°C, the temperature at which the net growth rate was a maximum, and it increased at lower and higher temperatures. Because the cells were grown on a 14:10 h light:dark cycle, if respiration rates had been the same in the light and dark, net growth would have become zero if the ratio in the light equaled $14/24 = 0.58$. The fact that the average ratio was 0.57 at 45°C suggests that dark respiration rates were smaller than light respiration rates.

The model (Appendix S1) indicated that allocations of carbon to the light reactions of photosynthesis (P/C) were greater under low irradiance than under high irradiance and greater under nutrient-replete conditions than under nitrate-limited conditions (12 of 12 comparisons, sign tests, $P = 0.03$; Fig. 6A). Allocations to E followed the opposite

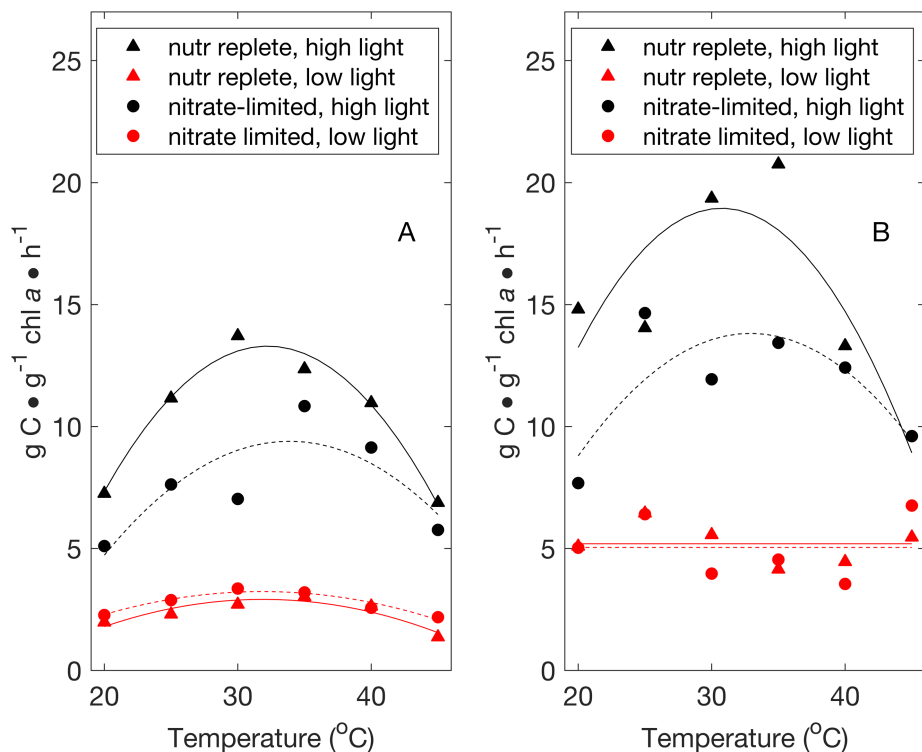


Fig. 4. Photosynthetic rates normalized to Chl *a* concentrations as functions of temperature, nutrient limitation, and irradiance. (A) Rates based on changes of particulate carbon concentrations in the growth chamber and calculated with Equation 3; (B) P_{\max}^* values (Equation 7) based on 5 min ^{14}C uptake experiments and calculated using Equation 6. Smooth curves are quadratic functions of temperature fit to the four data sets in panel A and to the high-light data in panel B. Horizontal lines in panel B are averages of the two low-light data sets.

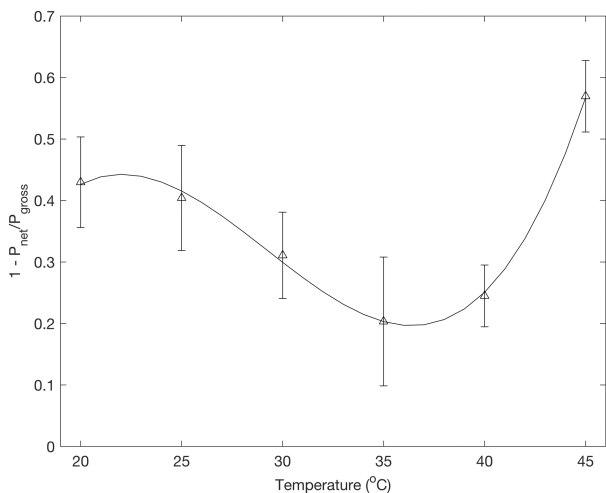


Fig. 5. Ratio of respiration to gross photosynthesis during the photoperiod versus temperature. Symbols are mean values, and error bars are standard errors of eight values corresponding to irradiances of 50 and 300 $\mu\text{mol photons} \cdot \text{m}^{-2} \cdot \text{s}^{-1}$, pCO_2 values of 400 and 1000 ppmv, and nitrate-limited and nutrient-replete conditions. The curve is a third-order polynomial fit to the data.

patterns (12 of 12 comparisons, sign tests, $P = 0.03$; Fig. 6B). Estimates of α based on model parameters (Appendix S1) and measured C:Chl *a* ratios (Fig. 6

C) were similar in magnitude to measured α values (Fig. 3) and were higher under high irradiance than under low irradiance and higher under nutrient-replete conditions versus nitrate-limited conditions (12 of 12 comparisons, sign tests, $P = 0.03$). The rate constant for the dark reactions of photosynthesis (K_E) was assumed to be independent of irradiance but varied with temperature by roughly a factor of 3 (Fig. 6D). The maximum and minimum values of K_E were $13 \cdot \text{d}^{-1}$ at 30°C and $3.7 \cdot \text{d}^{-1}$ at 20°C , respectively.

The ratio of carbon to Chl *a* in P (W_{Chl}) that produced a fit to the experimental C:Chl *a* ratios was similar at low and high irradiance under nutrient-replete conditions (Fig. 7A), was a maximum at a temperature of $\sim 30^\circ\text{C}$, and was higher at low irradiance than at high irradiance under nitrate-limited conditions (Fig. 7B). The experimental C:Chl *a* ratios (Fig. 7, C and D) were higher at high irradiance than at low irradiance (24 of 24 comparisons, sign test, $P = 0.03$), higher under nitrate-limited conditions than under nutrient-replete conditions (23 of 24 comparisons, sign test, $P = 0.03$), and, with the exception of the high-irradiance, nutrient-replete ratios, relatively insensitive to temperature.

The experimental C:N ratios were independent of temperature under both nutrient-replete (Fig. 8A)

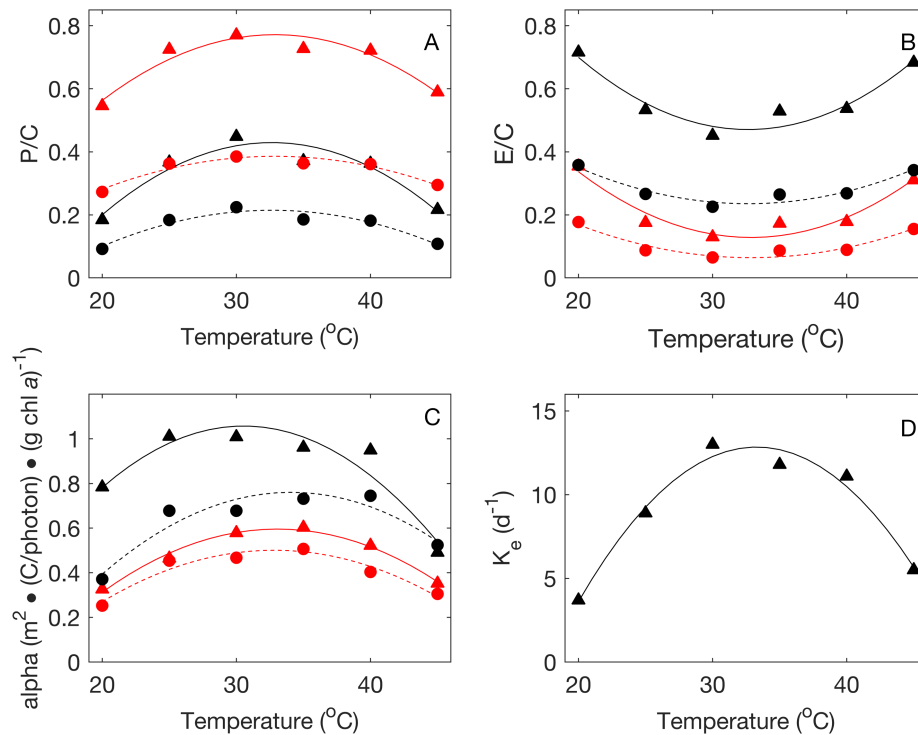


FIG. 6. Fractional allocations of cell carbon to P (panel A) and E (panel B), gross rate of photosynthesis per photon in limit of low irradiance normalized to experimental Chl *a* concentrations (panel C) based on model parameters (Supplementary Information) and rate constant (K_e) for dark reactions of photosynthesis (panel D). In panels A–C, solid lines indicate nutrient-replete conditions; dashed lines indicate nitrate-limited conditions; black lines and symbols indicate irradiance of $300 \mu\text{mol photons} \cdot \text{m}^{-2} \cdot \text{s}^{-1}$; and red lines and symbols indicate irradiance of $50 \mu\text{mol photons} \cdot \text{m}^{-2} \cdot \text{s}^{-1}$. The solid curves are 2nd-order polynomial fits to data.

and nitrate-limited (Fig. 8B) conditions, and they were higher under nitrate-limited conditions versus nutrient-replete conditions (24 of 24 comparisons, sign test, $P = 0.03$). The C:N ratios were higher under high irradiance than under low irradiance, but the difference was significant based on a paired *t*-test only under nutrient-replete conditions (4.88 versus $4.05 \text{ g} \cdot \text{g}^{-1}$; $P < 0.001$; Fig. 8A). Under nitrate-limited conditions, the C:N ratios averaged 6.89 and $6.56 \text{ g} \cdot \text{g}^{-1}$ (paired *t*-test, $P = 0.12$) at high and low irradiance, respectively (Fig. 8B). The model (Appendix S1) predicted no difference in C:N ratios under nutrient-replete conditions if the C:N ratios in P, E, and S were assumed to be identical. The best fit to the experimental data was obtained by assuming that the C:N ratios in S, P, and E (W_S , W_P , and W_E , respectively) were not identical and higher under nutrient-replete conditions. The best-fit values of W_S , W_P , and W_E were 6.1 , 3.6 , and $5.7 \text{ g} \cdot \text{g}^{-1}$, respectively, under nutrient-replete conditions and 3.5 , 3.5 , and $4.1 \text{ g} \cdot \text{g}^{-1}$, respectively, under nitrate-limited conditions. These values produced the lines in Figure 8, which gave a very good fit to both the nutrient-replete and nitrate-limited data.

The abundance of accessory pigments relative to Chl *a* differed markedly between cells growing under nitrate-limited versus nutrient-replete conditions (Fig. 9). The mean ratio of phycobilins to Chl

a under low-light, nutrient-replete conditions ($9.8 \text{ g} \cdot \text{g}^{-1}$) was at least twice the mean ratio under high-light, nutrient-replete conditions and under both low- and high-light, nitrate-limited conditions (one-way ANOVA, $F_{3,12} = 15.6$, $P = 0.0002$; Fig. 9A). Phycocyanin, rather than allophycocyanin, always comprised the majority of the phycobilins (90% on average). The ratio of total carotenoids to Chl *a* was roughly twofold greater in nitrate-limited versus nutrient-replete cells (nested ANOVA, $F_{1,2} = 55$, $P = 0.018$), but regardless of nutrient status, light intensity did not affect this ratio significantly (nested ANOVA, $F_{2,12} = 1.2$, $P = 0.32$; Fig. 9B).

DNA sequencing of the ITS region of CCMP 1629 yielded a sequence that was 1074 bp in length and had a GC content of 49%. This sequence has been deposited in the NCBI GenBank database and assigned the accession number [ON398846](https://www.ncbi.nlm.nih.gov/nuccore/ON398846). A search of the GenBank database revealed seven cyanobacterial strains that have >95% sequence identity and coverage with the ITS sequence of CCMP 1629 (Table 1). The sequence of the strain that was most similar (PCC 7003) was 98.9% identical to that of CCMP 1629 (12 mismatches) and had no gaps (i.e., 100% coverage; Fig. S4 in the Supporting Information). All seven of these strains were originally isolated from coastal environments, and all have been recently reclassified as members of the genus

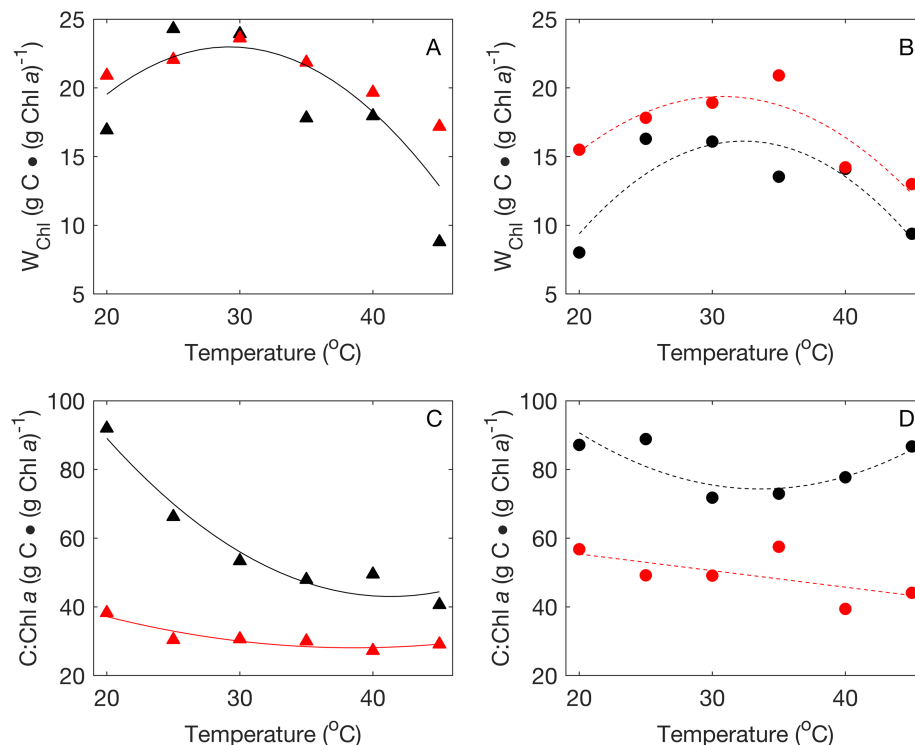


FIG. 7. Values of W_{Chl} that reproduce the experimental C:Chl a ratios given the P/C ratios (Fig. 5A) under nutrient-replete conditions (A) and nitrate-limited conditions (B). Black and red symbols correspond to high and low irradiance, respectively. Lines are quadratic polynomial functions of temperature fit to the W_{Chl} values. Panels C and D show the experimental C:Chl a ratios under nutrient-replete and nitrate-limited conditions, respectively. The smooth curves in panels C and D are low-order polynomials fit to the experimental data.

Limnotherix (Salazar et al. 2020). At least two of these genetically similar strains (PCC 7002 and PCC 11901) have been reported to grow very rapidly ($\sim 0.2\text{--}0.3 \cdot \text{h}^{-1}$) at 38°C under 1–3% CO_2 and constant illumination (Yu et al. 2015, Włodarczyk et al. 2020).

DISCUSSION

The evidence that increasing the pCO_2 enhances the growth rates of marine phytoplankton is mixed. Studies by Cassar et al. (2004) and Tortell et al. (2008a) have shown that direct uptake of bicarbonate accounts for $\sim 50\%$ and $\sim 80\%$, respectively, of inorganic carbon uptake by phytoplankton in the Southern Ocean. Thus, even in a part of the ocean where low temperatures enhance the solubility of CO_2 , direct uptake of bicarbonate still accounts for at least 50% of the inorganic carbon taken up by phytoplankton. Hein and Sand-Jensen (1997) have reported that along a transect in the Atlantic Ocean some algal communities responded positively to an increase of the pCO_2 to 855 ppmv, but the responses of primary production varied widely, from no response to more than a doubling. Tortell and Morel (2002) have reported no effect of variations in pCO_2 on phytoplankton growth rates in the eastern subtropical and equatorial Pacific Ocean, and Tortell et

al. (2008b) have reported either no effect or a 10% increase in primary production and growth rates of Southern Ocean phytoplankton in response to an increase in pCO_2 from 400 to 800 ppmv. Hopkinson et al. (2011) have argued on the basis of theoretical calculations that the energy savings associated with down-regulation of phytoplankton carbon concentrating mechanisms would increase primary production by only a few percent, and Goldman et al. (2017) have reported that neither pH nor pCO_2 measurably affect gross photosynthesis or respiration of the marine diatom *Thalassiosira weissflogii* over the range of pCO_2 and pH that is likely to characterize the ocean during the remainder of the twenty-first century.

Theoretical arguments suggest that increases in pCO_2 should lower the cost of inorganic carbon acquisition more for large cells than for small cells (Riebesell et al. 1993), and for this reason, cells as small as *Synechococcus* (0.6–2.0 μm) would be expected to benefit very little from an elevation of pCO_2 . Fu et al. (2007) have reported that raising the pCO_2 from 380 to 750 ppmv has no significant effect on the growth rate of *Synechococcus* CCMP 1334 at 20°C . Our results revealed a decrease in the growth rate of *S. elongatus* (CCMP 1629) when the pCO_2 was raised from 400 to 1000 ppmv in almost all cases. With the exception of the cells grown at high irradiance and 45°C , the nutrient-replete

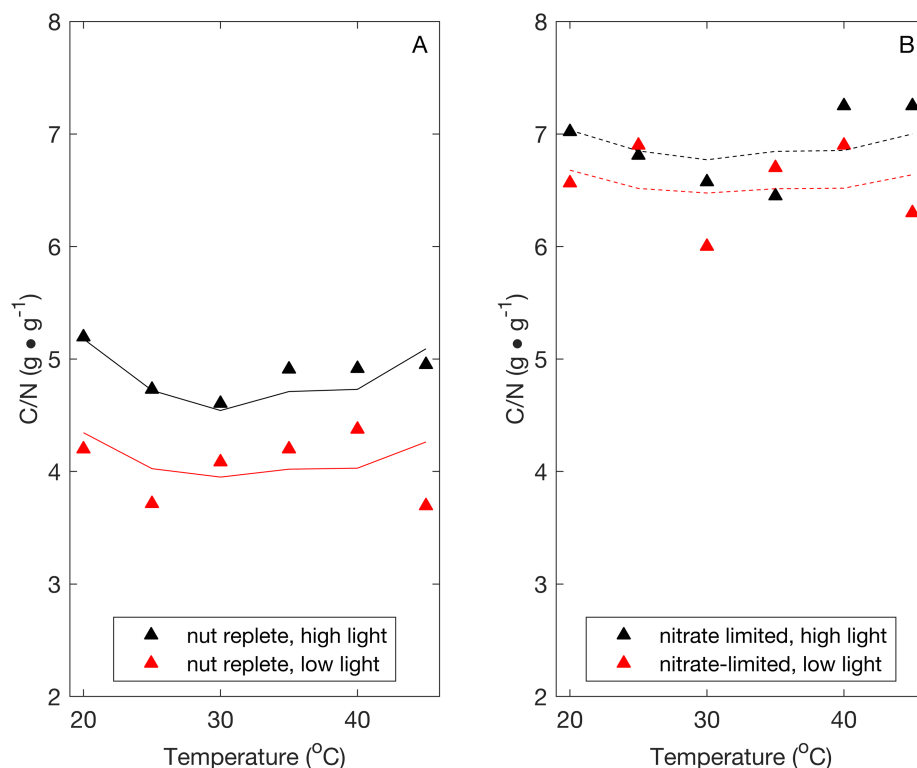


FIG. 8. C:N ratios as a function of temperature and irradiance under nutrient-replete conditions (A) and nitrate-limited conditions (B). Lines are model results.

growth rates at 1000 ppmv pCO₂ were about 8% lower than the corresponding growth rates at 400 ppmv pCO₂ at both high and low irradiance.

The 45% higher growth rate under nutrient-replete conditions, high irradiance, and 45°C at 1000 versus 400 ppmv pCO₂ suggests that the irradiance under these conditions was supraoptimal, because there was no similar response at low irradiance. The temperature of 45°C was clearly supraoptimal, and under these conditions, damage caused by photorespiration may have been greatly enhanced. The beneficial effect of increasing the pCO₂ may therefore have been the result of shifting the balance of competition between CO₂ and O₂ at the active sites of Rubisco.

The growth rates of CCMP 1629 were very similar to those of the genetically related *Synechococcus* clone PCC 7002, which has been reported to grow at $4.8 \cdot \text{d}^{-1}$ at 30°C (Bernstein et al. 2014). The temperature dependence of the nutrient-replete growth rates at high irradiance of CCMP 1629 (Fig. 1) is consistent with a Q₁₀ of 3.0–3.5, which is similar to the temperature dependence of K_E (Fig. 6D). CCMP 1629 and PCC 7002 grow much faster than most strains of marine *Synechococcus*, which grow no faster than $\sim 1.0\text{--}1.5 \cdot \text{d}^{-1}$ under optimal conditions (Agawin et al. 1998, Mackey et al. 2013). Indeed, the striking differences in maximum growth rate and temperature tolerance between strains of *Synechococcus* that are of coastal origin, such as PCC

7002, versus those of pelagic origin, such as WH 7805, may reflect the differences in ecotype and genetic lineage that have been reported between the two groups and that have prompted the recently proposed reclassification of PCC 7002 and WH 7805 into separate taxonomic orders (Salazar et al. 2020). Hence, it is important to acknowledge that the specific physiological responses of CCMP 1629 that we observed might not apply to pelagic strains.

The minimum quantum requirement for oxygen evolution in photosynthesis is 8–12 quanta (Hill and Govindjee 2014). It is likely that during our five-minute ¹⁴C uptake experiments, most of the ¹⁴C that was fixed was incorporated into sugars or polysaccharides (Halsey et al. 2011), for which the photosynthetic quotient (PQ) is 1.0 (Laws 1991). The minimum quantum requirement for short-term carbon fixation equals the quotient of the mean spectral extinction coefficient, \bar{k}_c , and α . Atlas and Bannister (1980) have estimated \bar{k}_c to be $14 \pm 2 \text{ m}^2 \cdot (\text{g Chl } a)^{-1}$ for a cyanobacterium (*Synechocystis*), as well as a chlorophyte (*Chlorella*) and diatom (*Navicula*). Assuming \bar{k}_c to be $14 \pm 2 \text{ m}^2 \cdot (\text{g Chl } a)^{-1}$ implies that α should be no greater than 1.17 ± 0.17 to $1.75 \pm 0.25 \text{ m}^2 \cdot \text{mol C} \cdot (\text{mol photons})^{-1} \cdot (\text{g Chl } a)^{-1}$. With one exception ($1.84 \text{ m}^2 \cdot \text{mol C} \cdot (\text{mol photons})^{-1} \cdot (\text{g Chl } a)^{-1}$ at 45°C and nutrient-replete conditions), all of our α values satisfied this constraint.

The principal accessory pigments in *Synechococcus* are zeaxanthin, β -carotene, and phycobilins.

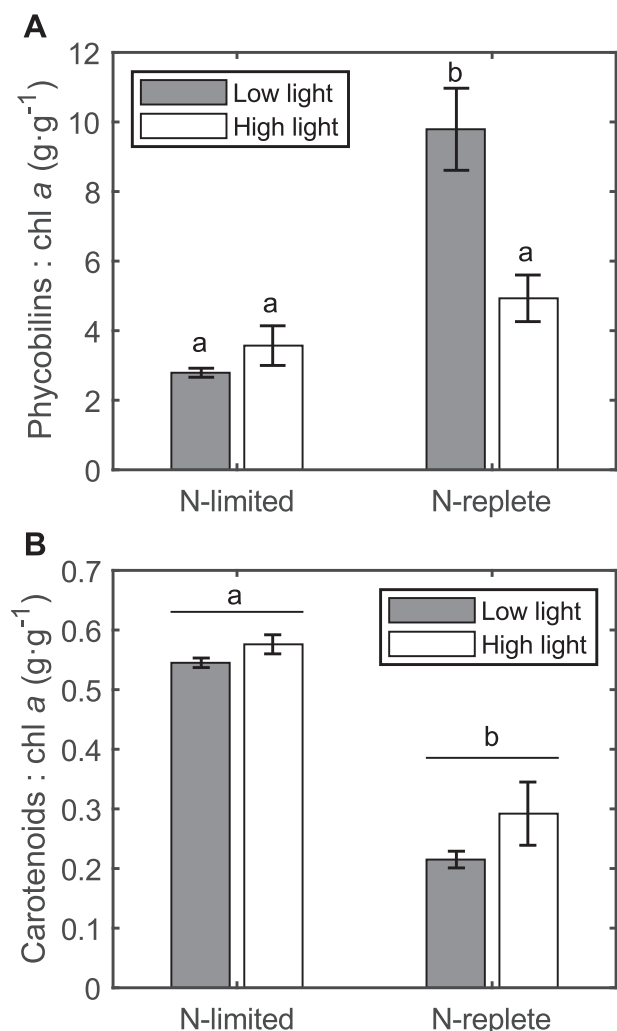


FIG. 9. Influence of nitrate limitation and/or light limitation on the mass ratios of (A) phycobilins to Chl *a* and (B) total carotenoids to Chl *a* in CCMP 1629 cultures growing at 25°C under 400 ppmv pCO₂. The phycobilins are the sum of the phycocyanin and allophycocyanin contents. Error bars are \pm standard error ($n = 3$ or 5). The different letters indicate statistically distinct groupings in: panel A, based on Tukey–Kramer HSD post hoc tests (ANOVA, $F_{3,12} = 15.6$, $P = 0.0002$; HSD, degrees of freedom = 12, $P < 0.003$); and in panel B, based on a nested ANOVA ($F_{1,2} = 55$, $P = 0.018$).

However, zeaxanthin is not a photosynthetic pigment in *Synechococcus* (Kana et al. 1988) and instead plays a photoprotective role (Bidigare et al. 1989), which may be particularly important under nutrient deprivation (Collier et al. 1994, Grossman et al. 1994). Nitrogen is required for the synthesis of phycocyanin but not β -carotene, and the content of phycocyanin in CCMP 1629 differed dramatically between nutrient-replete and nitrate-limited conditions (Fig. 9A). Although phycocyanin could be serving to some extent as a reserve of nitrogen, our observation that the phycobilin content relative to Chl *a* was greater at low versus high irradiance under nutrient-replete conditions is consistent with

phycocyanin's being photosynthetically active in CCMP 1629. The much greater phycocyanin content under nutrient-replete versus nitrate-limited conditions (Fig. 9A) may therefore account for the accordingly higher α values under nutrient-replete versus nitrate-limited conditions (Fig. 3B). The low value of α at 20°C and high irradiance, $0.53 \text{ m}^2 \cdot \text{mol C} \cdot (\text{mol photons})^{-1} \cdot (\text{g Chl } a)^{-1}$, likely reflects photooxidative damage. The temperature of 20°C was at least 10°C below the optimum temperature for growth of CCMP 1629, and at 20°C and an irradiance of $300 \mu\text{mol photons} \cdot \text{m}^{-2} \cdot \text{s}^{-1}$, nonphotochemical quenching by zeaxanthin may have been insufficient to prevent damage from reactive oxygen species. Oxidative stress at suboptimal temperatures may have been particularly great under nitrate-limited conditions and $300 \mu\text{mol photons} \cdot \text{m}^{-2} \cdot \text{s}^{-1}$. The average carotenoid-to-Chl *a* ratio at 25°C was greatest under nitrate-limited conditions and $300 \mu\text{mol photons} \cdot \text{m}^{-2} \cdot \text{s}^{-1}$, and under these same conditions at 20°C, the α averaged only $0.33 \text{ m}^2 \cdot \text{mol C} \cdot (\text{mol photons})^{-1} \cdot (\text{g Chl } a)^{-1}$. The absence of a similar depression of α at an irradiance of $50 \mu\text{mol photons} \cdot \text{m}^{-2} \cdot \text{s}^{-1}$ is consistent with the irradiance of $300 \mu\text{mol photons} \cdot \text{m}^{-2} \cdot \text{s}^{-1}$ being supraoptimal at 20°C under nitrate-limited conditions. The model, however, which made no allowance for supraoptimal irradiance, estimated that α would be consistently higher at high irradiance than at low irradiance at all temperatures (Fig. 7C). Although α was indeed higher at high irradiance at the three highest temperatures (Fig. 3A), it became increasingly lower at high irradiance versus low irradiance as the temperature was reduced from 30 to 20°C. The irradiance of $300 \mu\text{mol photons} \cdot \text{m}^{-2} \cdot \text{s}^{-1}$ thus appears to have become increasingly stressful as the temperature was reduced below the optimal temperature for growth of 35°C.

Falkowski (1981) has estimated the maximum possible assimilation number (Chl *a*-normalized rate of photosynthetic carbon fixation) of phytoplankton to be $24 \text{ g C} \cdot (\text{g Chl } a)^{-1} \cdot \text{h}^{-1}$ based on an assumed turnover time of 1 msec for a photosynthetic unit, an average photosynthetic unit size of 2000 Chl *a* molecules per O₂, and a PQ of 1.0 O₂ per CO₂. For growth on nitrate, the PQ is ~ 1.4 (Laws 1991), and the maximum assimilation number becomes $17 \text{ g C} \cdot (\text{g Chl } a)^{-1} \cdot \text{h}^{-1}$. Two considerations account for the differences between the data in Figure 4, A and B. The data in Figure 4B are based on 5 min ¹⁴C uptake and are therefore likely to be estimates of gross rather than net photosynthesis (Halsey et al. 2011), the products are likely sugars, and the PQ is therefore 1.0. The data in Figure 4A reflect net rather than gross photosynthesis, the products include proteins and lipids, and the associated PQ of 1.4 lowers the assimilation number by 40% compared to the assimilation number associated with the production of sugars and

TABLE 1. List of the cyanobacterial strains with ITS sequences that are >95% identical to that of CCMP 1629.

ITS region identity to CCMP 1629	Strain number	Originally isolated from ^a		Reclassified as ^b
		Environment	Location	
98.9%	PCC 7003	Clam bed (marine)	Connecticut, USA	<i>Limnothrix</i> sp.
98.0%	PCC 11901	Floating fish farm	Singapore	<i>Limnothrix euryhalinus</i>
98.0%	PCC 8807	Lagoon	Port Gentil, Gabon	<i>Limnothrix euryhalinus</i>
97.9%	PCC 73109	Coastal seawater	New York, USA	<i>Limnothrix euryhalinus</i>
97.7%	PCC 7117	Low-salinity brine pond	Western Australia	<i>Limnothrix euryhalinus</i>
97.6%	PCC 7002	Marine mud	Puerto Rico	<i>Limnothrix euryhalinus</i>
96.4%	NIES-970	Tidal mud flat	Japan	<i>Limnothrix</i> sp.

^aRippka et al. (1979), Richert et al. (2006), Shimura et al. (2017), Włodarczyk et al. (2020).

^bSalazar et al. (2020).

polysaccharides. The model of physiological acclimation by phytoplankton (Shuter 1979, Laws and Chalup 1990) accounts for the higher assimilation numbers and P_{\max}^* values of cells grown at 300 versus 50 $\mu\text{mol photons} \cdot \text{m}^{-2} \cdot \text{s}^{-1}$ based on a shift of resources from the light reactions to the dark reactions of photosynthesis to maximize growth rates as the irradiance is increased from 50 to 300 $\mu\text{mol photons} \cdot \text{m}^{-2} \cdot \text{s}^{-1}$. The greater allocation of cell carbon to the light and dark reactions of photosynthesis at 300 $\mu\text{mol photons} \cdot \text{m}^{-2} \cdot \text{s}^{-1}$ under nutrient-replete versus nitrate-limited conditions (Fig. 6, A and B) explains the higher assimilation numbers under nutrient-replete conditions (Fig. 4 A). A qualitatively similar difference in assimilation numbers would be expected at 50 $\mu\text{mol photons} \cdot \text{m}^{-2} \cdot \text{s}^{-1}$, and the results of the five min ^{14}C uptake experiments were consistent with that expectation (Fig. 4B). However, the assimilation numbers were consistently ~17% higher under nitrate-limited versus nutrient-replete conditions at 50 $\mu\text{mol photons} \cdot \text{m}^{-2} \cdot \text{s}^{-1}$ based on changes of PC concentrations (Fig. 4A). The likely explanation for this difference is that dark carbon loss rates were higher under nitrate-limited versus nutrient-replete conditions (Laws and Bannister 1980), and it was necessary for net photosynthetic rates during the photoperiod under nitrate-limited conditions to compensate for this greater loss of organic carbon at night. The irradiance of 50 $\mu\text{mol photons} \cdot \text{m}^{-2} \cdot \text{s}^{-1}$ was sufficiently close to the compensation irradiance that the difference in dark loss rates became significant.

Although productivity indices and P_{\max}^* values were consistently higher at high irradiance under nutrient-replete versus nitrate-limited conditions (Fig. 4), there was no difference in the analogous P_{\max}^* values at low irradiance, and the productivity indices were slightly higher under nitrate-limited conditions at low irradiance. The explanation is that the photosynthetic rate normalized to Chl *a* is the product of the growth rate and the C:Chl *a* ratio of the cells. The latter are negatively correlated with growth rates under nutrient-limited conditions (Laws and Bannister 1980). At low irradiance, the increase in the C:Chl *a* ratio almost exactly offset

the reduction in growth rate from nutrient-replete to nitrate-limited conditions. The result was productivity indices and P_{\max}^* values that were very insensitive to the degree of nutrient limitation at low irradiance.

The allocation of carbon resources in Figure 7, A–C is easily explained based on the assumptions of the model (Laws and Chalup 1990). Carbon is allocated to storage products only when growth rates are constrained by nutrient limitation, and the allocations are greater at high than at low irradiance and closely correlated with growth rates. The light reactions of photosynthesis were assumed to be independent of temperature, and to achieve a balance between the rates of the light and dark reactions, more carbon was allocated to the light reactions (Fig. 6A) when growth rates were high and the irradiance was low. The dark reactions were assumed to be temperature-dependent (Fig. 6D), and the allocation of carbon to the dark reactions (Fig. 6B) was therefore more or less a mirror image of the allocations to the light reactions. The Q_{10} associated with the dark reactions (Fig. 6D) was 3.5 and was therefore very similar to the Q_{10} of 3.2 for the respiration of planktonic foraminifera and their symbiotic algae (Lombard et al. 2009).

The values of W_{Chl} in Figure 7, A and B equal the corresponding P/C ratios in Figure 6A multiplied by the C:Chl *a* ratios in Figure 7, C and D, respectively, and are metrics of the size of the photosynthetic units in CCMP 1629. The principal antenna pigments involved in carbon fixation by CCMP 1629 are β -carotene and phycocyanin. There is little change in the cell quota of phycocyanin between low and high irradiance under nitrate-limited conditions because phycocyanin, which is a pigment–protein complex, requires nitrogen. The much larger W_{Chl} at low versus high irradiance under nitrate-limited conditions (Fig. 7B) can therefore be attributed to increases in the cell quota of β -carotene. The similarity of the W_{Chl} values at high and low irradiance under nutrient-replete conditions (Fig. 7, A and B) implies that the cells acclimated to changing irradiance under nutrient-replete conditions by changing the number (Fig. 6A) but not the size of

their photosynthetic units (Falkowski and Owens 1980). The larger W_{Chl} under nutrient-replete (Fig. 7A) versus nitrate-limited (Fig. 7B) conditions and the larger W_{Chl} at low versus high irradiance under nitrate-limited conditions (Fig. 7B) together imply that the photosynthetic antennae were larger (i.e., included phycocyanin) and more efficient in capturing photosynthetically active radiation under nutrient-replete conditions.

Goldman (1980) has argued that the C:N ratio of phytoplankton cells is a unique function of the ratio of their nutrient-limited growth rate to their nutrient-replete growth rate under otherwise identical conditions. We are aware of no study that has rigorously tested this hypothesis at different irradiances and over a wide range of temperatures. Our results (Fig. 8) revealed that the C:N ratios of CCMP 1629 were remarkably independent of temperature in the range 20–45°C at a fixed irradiance and relative growth rates of 1.0 and ~0.5 (paired *t*-test, $t_{11} = 2.8$, $P = 0.016$). The C:N ratios were, however, higher at high irradiance than at low irradiance at relative growth rates of both ~0.5 and 1.0, although the difference was significant (paired *t*-test, $t_{11} = 5.4$, $P < 0.05$) only in the latter case (Fig. 8A). This difference in C:N ratios was inconsistent with the relative growth rate hypothesis of Goldman (1980) and could be explained in the context of the Laws and Chalup (1990) model if the C:N ratios were not identical in S, P, and E and were systematically higher under nutrient-replete versus nitrate-limited conditions.

CONCLUSIONS

Our hypothesis that the nutrient-replete growth rates of *Synechococcus elongatus* would be unaffected by changing the $p\text{CO}_2$ from 400 ppmv to 1000 ppmv proved to be false. In all but one case, the growth rates were about 8% lower at 1000 ppmv $p\text{CO}_2$. The single exception was 45°C and high irradiance. In that case, growth rates were higher by about 45% at 1000 ppmv $p\text{CO}_2$, presumably because of photorespiratory effects at 400 ppmv $p\text{CO}_2$. Our hypothesis that any effects of $p\text{CO}_2$ on nutrient-replete growth rates would be independent of temperature and irradiance was therefore false. Our hypothesis that the physiological condition of *S. elongatus*, as evidenced by the initial slope and asymptote of short-term photosynthesis–irradiance curves, would be independent of temperature, irradiance, nutrient-limitation status, and $p\text{CO}_2$ was also false. The initial slopes were consistently higher under nutrient-replete versus nitrate-limited conditions, and although they were similar at high and low irradiance at most temperatures, they were significantly depressed at 20°C and high irradiance, presumably due to photorespiratory effects. P_{max}^* values were consistently higher at high versus low irradiance, and under high irradiance, they were

consistently higher under nutrient-replete versus nitrate-limited conditions. The hypothesis of Goldman (1980) that the C:N ratio would be a unique function of relative growth rate proved to be true with respect to temperature. However, under nutrient-replete conditions the C:N ratios were consistently ~17% lower at low irradiance versus high irradiance. The simple model of Laws and Chalup (1990) could explain this behavior if the C:N ratios in organic compounds allocated to structure and the light and dark reactions of photosynthesis were not identical and were higher under nutrient-replete conditions than under nitrate-limited conditions.

This work was supported by the National Science Foundation grant OCE 1536581 to E. A. L. We thank Dr. Scott Herke and the LSU Genomics Facility for assisting with the DNA sequencing work, and we thank Dr. David Hutchins and an anonymous reviewer for their constructive comments and suggestions for improving the original version of this manuscript.

AUTHOR CONTRIBUTIONS

E.A. Laws: Conceptualization (equal); formal analysis (equal); funding acquisition (equal); investigation (equal); methodology (equal); project administration (equal); supervision (lead); writing – original draft (equal). **S.A. McClellan:** Data curation (equal); investigation (equal); writing – review and editing (equal).

DATA AVAILABILITY STATEMENT

The data used to generate these results are available at www.bco-dmo.org/project/654347.

- Agawin, N. S. R., Duarte, C. M. & Agusti, S. 1998. Growth and abundance of *Synechococcus* sp. in a Mediterranean Bay: seasonality and relationship with temperature. *Mar. Ecol. Prog. Ser.* 170:45–53.
- Ahlgren, N. A. & Rocoap, G. 2012. Diversity and distribution of marine *Synechococcus*: multiple gene phylogenies for consensus classification and development of qPCR assays for sensitive measurement of clades in the ocean. *Front. Microbiol.* 3:213.
- Atlas, D. & Bannister, T. T. 1980. Dependence of mean spectral extinction coefficient of phytoplankton on depth, water color, and species. *Limnol. Oceanogr.* 25:157–9.
- Beardall, J., Stojkovic, S. & Larsen, S. 2009. Living in a high CO_2 world: impacts of global climate change on marine phytoplankton. *Plant Ecol. Divers.* 2:191–205.
- Bennett, A. & Bogorad, L. 1973. Complementary chromatic adaptation in a filamentous blue-green alga. *J. Cell Biol.* 58:419–35.
- Bernstein, H. C., Konopka, A., Melnicki, M. R., Hill, E. A., Kucek, L. A., Zhang, S. Y., Shen, G. Z., Bryant, D. A. & Beliaev, A. S. 2014. Effect of mono- and dichromatic light quality on growth rates and photosynthetic performance of *Synechococcus* sp. PCC 7002. *Front. Microbiol.* 5:488.
- Bigdare, R. R., Schofield, O. & Prezelin, B. B. 1989. Influence of zeaxanthin on quantum yield of photosynthesis of *Synechococcus* clone WH7803 (DC2). *Mar. Ecol. Prog. Ser.* 56:177–88.

- Breland, J. A. & Byrne, R. H. 1993. Spectrophotometric procedures for determination of sea-water alkalinity using bromocresol green. *Deep-Sea Res. Part I Oceanogr. Res. Pap.* 40:629–41.
- Cassar, N., Laws, E. A., Bidigare, R. R. & Popp, B. N. 2004. Bicarbonate uptake by Southern Ocean phytoplankton. *Global Biogeochem. Cycles* 18:1–18. <https://doi.org/10.1029/2003GB002116>.
- Collier, J. L., Herbert, S. K., Fork, D. C. & Grossman, A. R. 1994. Changes in the cyanobacterial photosynthetic apparatus during acclimation to macronutrient deprivation. *Photosynth. Res.* 42:173–83.
- Dickson, A. G., Sabine, C. L. & Christian, J. R. 2007. *Guide for Best Practices for Ocean CO₂ Measurements. PICES Special Publication 3*. North Pacific Marine Science Organization, Sidney, Canada 191 pp.
- EU 2011. *Guide to Best Practices for Ocean Acidification Research and Data Reporting*. European Union, Kiel, Germany 258 pp.
- Falkowski, P. G. 1981. Light-shade adaptation and assimilation numbers. *J. Plankton Res.* 3:203–16.
- Falkowski, P. G. & Owens, T. G. 1980. Light-shade adaptation: two strategies in marine phytoplankton. *Plant Physiol.* 66:592–5.
- Feng, Y. Y., Hare, C. E., Leblanc, K., Rose, J. M., Zhang, Y. H., DiTullio, G. R., Lee, P. A. et al. 2009. Effects of increased pCO₂ and temperature on the North Atlantic spring bloom. I. The phytoplankton community and biogeochemical response. *Mar. Ecol. Prog. Ser.* 388:13–25.
- Fu, F. X., Warner, M. E., Zhang, Y. H., Feng, Y. Y. & Hutchins, D. A. 2007. Effects of increased temperature and CO₂ on photosynthesis, growth, and elemental ratios in marine *Synechococcus* and *Prochlorococcus* (Cyanobacteria). *J. Phycol.* 43:485–96.
- Gao, K., Helbling, W. E., Haeder, D. P. & Hutchins, D. A. 2012a. Responses of marine primary producers to interactions between ocean acidification, solar radiation, and warming. *Mar. Ecol. Prog. Ser.* 470:167–89.
- Gao, K., Xu, J., Gao, G., Li, Y., Hutchins, D. A., Huang, B., Wang, L. et al. 2012b. Rising CO₂ and increased light exposure synergistically reduce marine primary productivity. *Nat. Clim. Change* 2:519–23.
- Goericke, R. & Repeta, D. J. 1992. The pigments of *Prochlorococcus marinus*: The presence of divinyl chlorophyll-*a* and chlorophyll-*b* in a marine prokaryote. *Limnol. Oceanogr.* 37:425–33.
- Goldman, J. A. L., Bender, M. L. & Morel, F. M. M. 2017. The effects of pH and pCO₂ on photosynthesis and respiration in the diatom *Thalassiosira weissflogii*. *Photosynth. Res.* 132:83–93.
- Goldman, J. C. 1980. Physiological processes, nutrient availability, and the concept of relative growth rate in marine phytoplankton ecology. In Falkowski, P. G. [Ed.] *Primary Productivity in the Sea*. Plenum, New York, pp. 179–94.
- Grossman, A. R., Schaefer, M. R., Chiang, G. G. & Collier, J. L. 1994. The responses of cyanobacteria to environmental conditions: light and nutrients. In Bryant, D. A. [Ed.] *The Molecular Biology of Cyanobacteria*. Springer, Dordrecht, pp. 641–75.
- Halsey, K. H., Milligan, A. J. & Behrenfeld, M. J. 2011. Linking time-dependent carbon-fixation efficiencies in *Dunaliella tertiolecta* (Chlorophyceae) to underlying metabolic pathways. *J. Phycol.* 47:66–76.
- Hein, M. & Sand-Jensen, K. 1997. CO₂ increases oceanic primary production. *Nature* 388:526–7.
- Hill, J. F. & Govindjee 2014. The controversy over the minimum quantum requirement for oxygen evolution. *Photosynth. Res.* 122:97–112.
- Holm-Hansen, O. & Riemann, B. 1978. Chlorophyll *a* determination: Improvements in methodology. *Oikos* 30:438–47.
- Hopkinson, B. M., Dupont, C. L., Allen, A. E. & Morel, F. M. M. 2011. Efficiency of the CO₂-concentrating mechanism of diatoms. *Proc. Natl. Acad. Sci. USA* 108:3830–7.
- Houghton, J. T., Ding, Y., Griggs, D. J., Noguier, M., Van der Linden, P. J., D'ai, X., Maskell, K. & Johnson, C. A. 2001. *Climate Change 2001: The Scientific Basis*. Cambridge University Press, Cambridge, UK 10 pp.
- Hutchins, D. A. & Fu, F. X. 2017. Microorganisms and ocean global change. *Nat. Microbiol.* 2:11.
- Kana, T. M., Glibert, P. M., Goericke, R. & Welschmeyer, N. A. 1988. Zeaxanthin and beta-carotene in *Synechococcus* WH7803 respond differently to irradiance. *Limnol. Oceanogr.* 33:1623–7.
- Laws, E. A. 1991. Photosynthetic quotients, new production and net community production in the open ocean. *Deep-Sea Res. Part I Oceanogr. Res. Pap.* 38:143–67.
- Laws, E. A. & Bannister, T. T. 1980. Nutrient- and light-limited growth of *Thalassiosira fluviatilis* in continuous culture, with implications for phytoplankton growth in the ocean. *Limnol. Oceanogr.* 25:457–73.
- Laws, E. A. & Chalup, M. S. 1990. A microalgal growth model. *Limnol. Oceanogr.* 35:597–608.
- Laws, E. A., McClellan, S. A. & Passow, U. 2020. Interactive effects of CO₂, temperature, irradiance, and nutrient limitation on the growth and physiology of the marine diatom *Thalassiosira pseudonana* (Coscinodiscophyceae). *J. Phycol.* 56:1614–24.
- Li, F. T., Beardall, J., Collins, S. & Gao, K. S. 2017. Decreased photosynthesis and growth with reduced respiration in the model diatom *Phaeodactylum tricorutum* grown under elevated CO₂ over 1800 generations. *Glob. Chang. Biol.* 23:127–37.
- Li, W. K. W. 1994. Primary production of prochlorophytes, cyanobacteria, and eukaryotic ultraphytoplankton: measurements from flow cytometric sorting. *Limnol. Oceanogr.* 39:169–75.
- Lombard, F., Erez, J., Michel, E. & Labeyrie, L. 2009. Temperature effect on respiration and photosynthesis of the symbiont-bearing planktonic foraminifera *Globigerinoides ruber*, *Orbulina universa*, and *Globigerinella siphonifera*. *Limnol. Oceanogr.* 54:210–8.
- Mackey, K. R. M., Paytan, A., Caldeira, K., Grossman, A. R., Moran, D., McIlvin, M. & Saito, M. A. 2013. Effect of temperature on photosynthesis and growth in marine *Synechococcus* spp. *Plant Physiol.* 163:815–29.
- Moore, L. R., Goericke, R. & Chisholm, S. W. 1995. Comparative physiology of *Synechococcus* and *Prochlorococcus*: Influence of light and temperature on growth, pigments, fluorescence and absorptive properties. *Mar. Ecol. Prog. Ser.* 116:259–75.
- Nicholas, K. B. & Nicholas, H. B. 1997. GeneDoc: a tool for editing and annotating multiple sequence alignments. Distributed by the authors. <https://nrbsc.org/gfx/genedoc/>.
- Partensky, F., Blanchot, J. & Vault, D. 1999a. Differential distribution and ecology of *Prochlorococcus* and *Synechococcus* in oceanic waters: a review. In Charpy, L. & Larkum, A. W. D. [Eds.] *Marine Cyanobacteria. Bulletin de l'Institut Oceanographique*. L'Institut Oceanographique de Monaco, Monaco, pp. 457–75.
- Partensky, F., Hess, W. R. & Vault, D. 1999b. *Prochlorococcus*, a marine photosynthetic prokaryote of global significance. *Microbiol. Mol. Biol. Rev.* 63:106–27.
- Popp, B. N., Laws, E. A., Bidigare, R. R., Dore, J. E., Hanson, K. L. & Wakeham, S. G. 1998. Effect of phytoplankton cell geometry on carbon isotopic fractionation. *Geochim. Cosmochim. Acta* 62:69–77.
- Richert, L., Golubic, S., Le Guedes, R., Herve, A. & Payri, C. 2006. Cyanobacterial populations that build 'kopara' microbial mats in Rangiroa, Tuamotu Archipelago, French Polynesia. *Eur. J. Phycol.* 41:259–79.
- Riebesell, U., Wolfgladrow, D. A. & Smetacek, V. 1993. Carbon dioxide limitation of marine phytoplankton growth rates. *Nature* 361:249–51.
- Rippka, R., Deruelles, J., Waterbury, J. B., Herdman, M. & Stanier, R. Y. 1979. Generic assignments, strain histories and properties of pure cultures of Cyanobacteria. *J. Gen. Microbiol.* 111:1–61.
- Robbins, L. L., Hansen, M. E., Kleypas, J. A. & Meylan, S. C. 2010. CO₂calc: a user-friendly seawater carbon calculator for Windows, Mac OS X, and iOS (iPhone). Open-File Report, Reston, VA.
- Rocap, G., Distel, D. L., Waterbury, J. B. & Chisholm, S. W. 2002. Resolution of *Prochlorococcus* and *Synechococcus* ecotypes by

- using 16S-23S ribosomal DNA internal transcribed spacer sequences. *Appl. Environ. Microbiol.* 68:1180–91.
- Rost, B., Zondervan, I. & Wolf-Gladrow, D. 2008. Sensitivity of phytoplankton to future changes in ocean carbonate chemistry: current knowledge, contradictions and research directions. *Mar. Ecol. Prog. Ser.* 373:227–37.
- Ruan, Z. X., Prasil, O. & Giordano, M. 2018. The phycobilisomes of *Synechococcus* sp. are constructed to minimize nitrogen use in nitrogen-limited cells and to maximize energy capture in energy-limited cells. *Environ. Exp. Bot.* 150:152–60.
- Salazar, V. W., Tschoeke, D. A., Swings, J., Cosenza, C. A., Matoso, M., Thompson, C. C. & Thompson, F. L. 2020. A new genomic taxonomy system for the *Synechococcus* collective. *Environ. Microbiol.* 22:4557–70.
- Shimura, Y., Hirose, Y., Misawa, N., Wakazuki, S., Fujisawa, T., Nakamura, Y., Kanesaki, Y., Yamaguchi, H. & Kawachi, M. 2017. Complete genome sequence of a coastal Cyanobacterium, *Synechococcus* sp. Strain NIES-970. *Microbiol. Resour. Ann.* 5:e00139-17.
- Shuter, B. 1979. A model of physiological adaptation in unicellular algae. *J. Theor. Biol.* 78:519–52.
- Sohm, J. A., Ahlgren, N. A., Thomson, Z. J., Williams, C., Moffett, J. W., Saito, M. A., Webb, E. A. & Rocab, G. 2016. Co-occurring *Synechococcus* ecotypes occupy four major oceanic regimes defined by temperature, macronutrients and iron. *ISME J.* 10:333–45.
- Strickland, J. D. H. & Parsons, T. R. 1972. *A Practical Handbook of Seawater Analysis*. Fisheries Research Board of Canada, Ottawa, 310 pp.
- Sunda, W. G. & Hardison, D. R. 2007. Ammonium uptake and growth limitation in marine phytoplankton. *Limnol. Oceanogr.* 52:2496–506.
- Tortell, P. D. & Morel, F. M. M. 2002. Sources of inorganic carbon for phytoplankton in the eastern Subtropical and Equatorial Pacific Ocean. *Limnol. Oceanogr.* 47:1012–22.
- Tortell, P. D., Payne, C., Gueguen, C., Strzepak, R. F., Boyd, P. W. & Rost, B. 2008a. Inorganic carbon uptake by Southern Ocean phytoplankton. *Limnol. Oceanogr.* 53:1266–78.
- Tortell, P. D., Payne, C. D., Li, Y. Y., Trimbom, S., Rost, B., Smith, W. O., Riesselman, C., Dunbar, R. B., Sedwick, P. & DiTullio, G. R. 2008b. CO₂ sensitivity of Southern Ocean phytoplankton. *Geophys. Res. Lett.* 35:5.
- Veldhuis, M. J. W., Kraay, G. W., VanBleijswijk, J. D. L. & Baars, M. A. 1997. Seasonal and spatial variability in phytoplankton biomass, productivity and growth in the northwestern Indian Ocean: the southwest and northeast monsoon, 1992–1993. *Deep-Sea Res. Part I Oceanogr. Res. Pap.* 44:425–49.
- Wlodarczyk, A., Selao, T. T., Norling, B. & Nixon, P. J. 2020. Newly discovered *Synechococcus* sp. PCC 11901 is a robust cyanobacterial strain for high biomass production. *Commun. Biol.* 3:215. <https://doi.org/10.1038/s42003-020-0910-8>
- Yool, A., Popova, E. E., Coward, A. C., Bernie, D. & Anderson, T. R. 2013. Climate change and ocean acidification impacts on lower trophic levels and the export of organic carbon to the deep ocean. *Biogeosciences* 10:5831–54.
- Yu, J. J., Liberton, M., Cliften, P. F., Head, R. D., Jacobs, J. M., Smith, R. D., Koppelaar, D. W., Brand, J. J. & Pakrasi, H. B. 2015. *Synechococcus elongatus* UTEX 2973, a fast growing cyanobacterial chassis for biosynthesis using light and CO₂. *Sci. Rep.* 5:10.
- Zeebe, R. E. & Wolf-Gladrow, D. 2001. *CO₂ in Seawater: Equilibrium, Kinetics, Isotopes*. Elsevier, Amsterdam, Netherlands 346 pp.
- Zwirgmaier, K., Jardillier, L., Ostrowski, M., Mazard, S., Garczarek, L., Vault, D., Not, F., Massana, R., Ulloa, O. & Scanlan, D. J. 2008. Global phylogeography of marine *Synechococcus* and

Prochlorococcus reveals a distinct partitioning of lineages among oceanic biomes. *Environ. Microbiol.* 10:147–61.

Supporting Information

Additional Supporting Information may be found in the online version of this article at the publisher's web site:

Appendix S1. Details of continuous culture methodology, theoretical model of phytoplankton growth, DNA sequencing methods, and summary of results.

Figure S1. Double-walled polycarbonate growth chamber with culture of *Synechococcus elongatus*. The working volume of the growth chamber is determined by the position of the overflow tube, which in this picture had not yet been incorporated into the design.

Figure S2. Diagram of the chemostat with three-way valve for bubbling air and collecting samples.

Figure S3. Estimated photosynthetic rate from 5 min uptake of ¹⁴C of treatment at 25°C, 50 μmol photons · m⁻² · s⁻¹, 1000 ppm pCO₂, and nutrient-replete conditions, at the end of the photoperiod. The smooth curve is a hyperbolic tangent fit to the data by least squares.

Figure S4. Alignment of the seven sequences that are >95% identical to the CCMP 1629 ITS sequence (16S-1247 23S-241) according to a GenBank BLAST query. Red vertical lines indicate base mismatches in a sequence relative to the CCMP 1629 sequence; blue vertical lines indicate gaps in a sequence relative to the CCMP 1629 sequence. The first column lists the accession number of each aligned sequence. The three rightmost columns list the % identity, % coverage, and number of base mismatches from left to right, respectively. The image of the alignments was generated by the NCBI Multiple Sequence Alignment Viewer (v. 1.22).

Table S1. Characteristics of seawater with a total alkalinity of 2365 μeq · L⁻¹ as a function of pCO₂ and temperature based on equations in Zeebe and Wolf-Gladrow, CO₂ in Seawater: Equilibrium, Kinetics, Isotopes (2001).

Table S2. Summary of experimental results of continuous culture studies of *Synechococcus* CCMP 1629.